# Uncertainty Quantification and Measurement Error Correlation in Linear State Estimation

Ginevra Larroux
*École polytechnique fédérale de Lausanne*
Lausanne, Switzerland

Dmitry Shchetinin
*Hitachi Energy Research*
Baden-Daettwil, Switzerland

***Abstract*—The linearity of the measurement model in Phasor-Measurement-Unit-observable grids makes state estimation a convex optimization problem that can be solved with very low latency in real time. However, state-of-the-art Linear State Estimation (LSE) implementations often rely on simplified noise models to preserve computational efficiency, at the cost of reduced estimation accuracy, and typically provide outputs limited to point estimates, without a statistical quantification of their uncertainty. This paper addresses these limitations by introducing a general LSE framework that (i) embeds experimentally validated synchrophasor error statistics through a non-diagonal measurement error covariance matrix, and (ii) computes confidence intervals for the estimated state by leveraging intermediate results from the LSE solution procedure with marginal added computational cost. The method is validated on networks of various sizes, demonstrating scalability, improved accuracy and reliability of the estimates.**

***Index Terms*—power system state estimation, uncertainty quantification, measurement noise modeling**

## I. Introduction

System operators rely on State Estimation (SE) for grid monitoring and control. The estimator reconstructs the system state from time-aligned field measurements of voltage and current (phasors from Phasor Measurement Units (PMUs), or magnitude-only from Remote Terminal Units (RTUs)). The choice of estimator is driven by the available measurements and process model, reporting rate, latency of the communication layer, and performance requirements in terms of accuracy, computational efficiency, and robustness to bad data [1, 2]. Modern power systems exhibit faster dynamics due to inverter-interfaced renewable generation, making fast estimators suitable for real-time operation increasingly important. In PMU-observable grids, the mapping between synchrophasor measurements and the system state in rectangular coordinates is linear, yielding the convex Linear State Estimation (LSE) problem (quadratic under Least Squares (LS)), which can be solved efficiently. Although full PMU-observability is not yet achieved across all transmission networks, the industry is moving in that direction; motivated by this trend, this paper proposes a method that improves the accuracy and statistical consistency of LSE while preserving computational efficiency compatible with real-time applications.

A key limitation of state-of-the-art LSE lies in the adopted synchrophasor noise models. Synchrophasors are the output of a measurement chain including Instrument Transformers (ITs), sampling and digitization, and PMU computation, each contributing to the overall uncertainty through both systematic and random errors [3]. Experimental characterizations of ITs indicate that their contribution is predominantly systematic and, in principle, accountable [4–7]; Current Transformers (CTs) and Voltage Transformers (VTs) standards [8] specify limits for ratio and phase-angle errors. For class M PMUs, standards define accuracy through a guaranteed Total Vector Error (TVE) [9], which bounds the combined magnitude and phase error within a circle in the complex plane centered at the true phasor. Experimental evidence and manufacturer datasheets indicate that phase errors are typically much smaller than magnitude errors and that both error distributions are concentrated around zero or small biases [10, 11]. Under steady-state conditions, a Gaussian model for magnitude and phase errors (with distinct variances and negligible correlation) provides the standard baseline in instrument characterization. Reported non-Gaussian fits from field data often arise when errors are aggregated across different operating conditions and nonstationary regimes [12]. By contrast, controlled laboratory experiments, on commercial PMUs [10, 13], under steady-state conditions, found no evidence to reject Gaussianity for magnitude errors and only limited evidence against it for phase errors, the latter depending strongly on the device's time-synchronization, internal clock properties, and the presence of interfering components. Hence, Gaussianity remains the most reasonable and practical hypothesis for the random error contribution of the measurement chain. Despite these considerations, LSE implementations frequently assume noise statistics invariant with operating conditions [2, 14, 15]; and even when variances are scaled with the measurand magnitude, they often neglect the correlation between real and imaginary components induced when transforming Gaussian magnitude and phase errors to rectangular coordinates [1]. These simplifications are primarily motivated by computational constraints: moving from a diagonal to a non-diagonal covariance matrix substantially increases the cost of the required linear-algebra operations, often making it incompatible with real-time operation.

This also explains why uncertainty quantification for the reconstructed state remains limited. While bad-data detection and robust estimation have been studied extensively, providing confidence intervals (CIs) is comparatively underexplored [16, 17]. In order to retain CIs' statistical significance, the measurement error covariance matrix cannot be approximated as described above, and standard Cholesky or lower-upper (LU) factorization cannot be used to invert it as they do not provide the specific inverse entries required to compute variances of bus-voltage estimates (and derived quantities) across LSE formulations (see Section II-B). Consequently, such computations are typically not achievable in real time. Existing works either model uncertainty through deterministic error bounds reflecting meter accuracies [18, 19], or focus on how to additionally integrate uncertainty of pseudo-measurements and grid parameters in SE without extending to rectangular coordinates (see Section II-A) [20, 21]. Moreover, the scalability of these approaches with network size is in

979-8-3315-8138-1

general not demonstrated, and the associated computational complexity not addressed.

To address these limitations, this paper develops a general framework for solving different formulations of the LSE problem under the hypothesis of i.i.d. gaussian *magnitude* and *phase* errors with *distinct* standard deviations, and accounting for the projected noise correlation in rectangular coordinates, while preserving convexity. Intermediate results from the matrix inversion procedure that solves the linear system of Karush–Kuhn–Tucker (KKT) optimality conditions are leveraged to compute the CIs for the state estimates (bus voltage phasors) and derived quantities (branch currents and power flows). Computational efficiency is ensured by tailoring sparse linear-algebra routines to compute only the relevant subsets of the matrix inverse required for variance evaluation. The proposed estimator is tested on systems ranging from 118 to 10,000 buses, demonstrating scalability, improved accuracy and statistical consistency, and computation times compatible with real-time operation.

## II. Linear State Estimation Formulation

### A. LSE optimization problem

For a PMU-observable system, the LS LSE optimization problem is formulated in complex coordinates as

$$\begin{aligned} &\underset{v,e}{\text{minimize}} && e^\dagger \Omega^{-1} e && \text{(1a)}\\ &\text{subject to} && Hv + e = z, && \text{(1b)}\end{aligned}$$

where $v \in \mathbb{C}^n$ denotes the states variables (bus voltages), $z \in \mathbb{C}^m$ the measurements (voltage and current phasors), $H \in \mathbb{C}^{m\times n}$ the linear measurement model, $e \in \mathbb{C}^m$ the vector of residuals, and $\Omega \in \mathbb{R}^{m\times m}$ the measurement error covariance matrix. $(\cdot)^\dagger$ is the conjugate transpose operator. Problem (1) can be equivalently reformulated in the domain of reals (2), which allows modeling distinct standard deviations for the real and imaginary parts of the measurement error, and their covariance. Let $v_\Re, v_\Im \in \mathbb{R}^n$ denote the real and imaginary parts of $v$, $e_\Re, e_\Im \in \mathbb{R}^m$ denote the real and imaginary parts of $e$, and $\Omega_{\Re\Im} \in \mathbb{R}^{2m\times 2m}$ denote the covariance matrix in rectangular coordinates.

$$\begin{aligned} &\underset{v_\Re, v_\Im, e_\Re, e_\Im}{\text{minimize}} && [e_\Re, e_\Im]\Omega_{\Re\Im}^{-1}[e_\Re, e_\Im]^T && \text{(2a)}\\ &\text{subject to} && \Re(H)v_\Re - \Im(H)v_\Im + e_\Re = \Re(z) && \text{(2b)}\\ & && \Im(H)v_\Re + \Re(H)v_\Im + e_\Im = \Im(z), && \text{(2c)}\end{aligned}$$

with $\Re(\cdot)$, $\Im(\cdot)$ real and imaginary operators.

### B. Commonly used formulations of LSE problem

The three commonly used formulations of the LSE problem [22] are recalled here, in complex form, as the proposed method for quantifying state uncertainty differs across them. These vary in how the "known" zero-injection bus constraints (whose corresponding equations should exhibit zero mismatches at optimality) are incorporated, and in the optional use of auxiliary variables. In the order presented, the associated linear systems of equations corresponding to the KKT conditions increase in size, while exhibiting improved numerical conditioning.

Let $H_1 \in \mathbb{C}^{m_1\times n}$ include both single-element measurement equations and bus balances with nonzero-current injections, $z_1 \in \mathbb{C}^{m_1}$ denote the corresponding phasor measurements, and $\Omega_1 \in \mathbb{C}^{m_1\times m_1}$ correspondent covariance matrix. Further, let $H_2 \in \mathbb{C}^{m_2\times n}$ denote the matrix mapping bus voltages to the zero-current bus balance equations. By construction, $H := \begin{bmatrix} H_1 \\ H_2 \end{bmatrix}$, and $z := \begin{bmatrix} z_1 \\ 0 \end{bmatrix}$.

1) Unconstrained optimization problem

$$\underset{v}{\text{minimize}} \quad (Hv - z)^\dagger \Omega^{-1}(Hv - z), \tag{3}$$

where $\Omega := \begin{pmatrix} \Omega_1 & 0 \\ 0 & \Omega_2 \end{pmatrix}$, and $\Omega_2 \in \mathbb{C}^{m_2\times m_2}$ is a diagonal matrix whose entries are artificially small constants, representing a low degree of uncertainty.

The system of KKT optimality conditions is

$$(H^\dagger \Omega^{-1} H)v = H^\dagger \Omega^{-1} z. \tag{4}$$

2) Constrained optimization problem

$$\begin{aligned} &\underset{v,\lambda}{\text{minimize}} && (z_1 - H_1 v)^\dagger \Omega_1^{-1}(z_1 - H_1 v) && \text{(5a)}\\ &\text{subject to} && H_2 v = 0. && \text{(5b)}\end{aligned}$$

The system of KKT optimality conditions, with the dual variable $\lambda \in \mathbb{C}^{m_2}$ is

$$\begin{bmatrix} H_1^\dagger \Omega_1^{-1} H_1 & H_2^\dagger \\ H_2 & 0 \end{bmatrix} \begin{bmatrix} v \\ \lambda \end{bmatrix} = \begin{bmatrix} H_1^\dagger \Omega_1^{-1} z_1 \\ 0 \end{bmatrix}. \tag{6}$$

3) Augmented optimization problem

$$\begin{aligned} &\underset{v,\lambda,r}{\text{minimize}} && r^\dagger \Omega_1^{-1} r && \text{(7a)}\\ &\text{subject to} && H_1 v - r = z_1 && \text{(7b)}\\ & && H_2 v = 0. && \text{(7c)}\end{aligned}$$

The system of KKT optimality conditions, with the dual variables $\lambda \in \mathbb{C}^{m_2}, \mu \in \mathbb{C}^{m_1}$ is

$$\begin{bmatrix} 0 & H_2^\dagger & H_1^\dagger \\ H_2 & \Omega_1 & 0 \\ H_1 & 0 & 0 \end{bmatrix} \begin{bmatrix} v \\ \lambda \\ \mu \end{bmatrix} = \begin{bmatrix} 0 \\ z_1 \\ 0 \end{bmatrix}. \tag{8}$$

The optimization problems in (3), (5), and (7) are solved as linear systems $Ax = b$, respectively defined in (4), (6), and (8).

## III. Proposed method

### A. Measurement error model

This paper models the *magnitude* and *phase* errors as independent, zero-mean normal variables with distinct standard deviations. Figure 1 compares the joint probability distribution function (pdf) of the proposed noise model (right) with that of the conventional model (left), which assumes independent, normally distributed *real* and *imaginary* components of phasor measurement errors, with equal standard deviations.

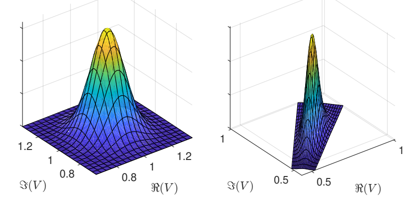


Fig. 1: Noise model. I.i.d. *real* and *imaginary* parts (left), i.i.d. *magnitude* and *phase* (right) of phasor measurement error.

Let the magnitude and phase of a complex measurement $\bar{Z}_m$ and its corresponding true value $\bar{Z}_t$ be defined respectively as $Z_m := |\bar{Z}_m|$, $\theta_m := \angle \bar{Z}_m$ and $Z_t$, $\theta_t$. Their pdfs are $Z_m \sim \mathcal{N}(Z_t, \sigma_Z) =: f_Z(Z_m)$ and $\theta_m \sim \mathcal{N}(\theta_t, \sigma_\theta) =: f_\theta(\theta_m)$. Define the real and imaginary parts of the complex

979-8-3315-8138-1

measurement as $Z_m^{'}$ and $Z_m^{''}$. The expected value, variance, and covariance of the normal pdfs in rectangular coordinates can be derived, from statistical theory. For brevity, only the covariance $\mathrm{cov}\big[Z_m^{'}, Z_m^{''}|Z_t, \theta_t\big] =: \Sigma$ expression is presented,

$$\Sigma = \mathrm{E}\big[Z_m^{'} Z_m^{''}|Z_t, \theta_t\big] - \mathrm{E}\big[Z_m^{'}|Z_t, \theta_t\big] \cdot \mathrm{E}\big[Z_m^{''}|Z_t, \theta_t\big]. \quad (9)$$

Observe that (9) includes the *true values* of the measured quantities, which are however not available in practice. Therefore, as done in [23], the *expected value* of the variances and covariance conditioned on the *measured quantities* $\mathrm{E}\left[\mathrm{cov}\left[Z_m^{'}, Z_m^{''}|Z_t, \theta_t\right] \big| Z_m, \theta_m\right] =: \Sigma_m$ is considered,

$$\begin{aligned} \Sigma_m &= \Sigma \int_{-\infty}^{\infty} f_Z(Z_m) dZ_m \int_{-\infty}^{\infty} f_\theta(\theta_m) d\theta_m \\ &= \frac{1}{2} \sin(2\theta_m) e^{-4\sigma_\theta^2} \left( \left(Z_m^2 + \sigma_Z^2\right)\left(1 - e^{\sigma_\theta^2}\right) + \sigma_Z^2 \right). \end{aligned} \quad (10)$$

Note that (10) is an algebraic expression that can be evaluated in a pre-processing step. Figure 2 illustrates the resulting variances of the real and imaginary parts of the measurements, and their covariance. All quantities vary periodically as a function of the measurement phase. As the relative difference between magnitude and phase accuracy increases, the correlation between the real and imaginary components of the measurement error becomes more pronounced, as indicated by the progression from the yellow to the red to the blue solid line. Furthermore, the variances (black lines) are of the same order of magnitude as the peaks of the covariance function (colored lines), most noticeably for $\sigma_\theta = 1\,\mathrm{mrad}$ (blue line).

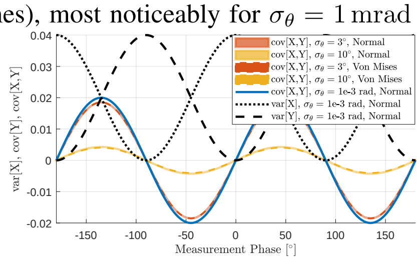


Fig. 2: Variance of the real and the imaginary parts of the measurement errors (black) and their covariance (colored) as a function of the measurement phase. Variable $\sigma_\theta$, constant $\sigma_Z = 1\%$ of the rated magnitude.

### *B. Linear state estimation with proposed error model*

The measurement error covariance matrix in rectangular coordinates $\Omega_{\Re\Im} \in \mathbb{R}^{2m \times 2m}$ is structured as follows,

$$\Omega_{\Re\Im} = \begin{pmatrix} \mathrm{diag}(\sigma_{\Re\Re}) & \mathrm{diag}(\sigma_{\Re\Im}) \\ \mathrm{diag}(\sigma_{\Im\Re}) & \mathrm{diag}(\sigma_{\Im\Im}) \end{pmatrix}, \quad (11)$$

with $\sigma_{\Re\Re} := (\sigma_{\Re_i\Re_i})_{i=1}^m \in \mathbb{R}^m$, $\sigma_{\Im\Im} := (\sigma_{\Im_i\Im_i})_{i=1}^m \in \mathbb{R}^m$ variances and $\sigma_{\Re\Im} = \sigma_{\Im\Re} := (\sigma_{\Re_i\Im_i})_{i=1}^m \in \mathbb{R}^m$ covariances, given the convention $\sigma_{\Re_i\Im_j} = \mathrm{cov}[e_{\Re_i}, e_{\Im_j}]$. Given the sparsity pattern of (11), its inverse can be constructed as follows,

$$\Omega_{\Re\Im}^{-1} = \begin{pmatrix} +W\,\mathrm{diag}(\sigma_{\Im\Im}) & -W\,\mathrm{diag}(\sigma_{\Re\Im}) \\ -W\,\mathrm{diag}(\sigma_{\Re\Im}) & +W\,\mathrm{diag}(\sigma_{\Re\Re}) \end{pmatrix}, \quad (12)$$

where $W \in \mathbb{R}^{m \times m}$ is a diagonal matrix given by

$$W := \mathrm{diag}\left( \frac{1}{\sigma_{\Re_i\Re_i}\sigma_{\Im_i\Im_i} - \sigma_{\Re_i\Im_i}^2} \right)_{i=1}^m \in \mathbb{R}^m. \quad (13)$$

The precision matrix $\Omega_{\Re\Im}^{-1}$ is positive definite and non-diagonal by construction, thus Generalized Least Squares (GLS) is required.

### *C. Uncertainty quantification of obtained results*

State estimates CIs are constructed from their covariance matrix. The CIs include, by definition, values not statistically different from the estimate at a user-defined significance level, allowing inference about the true parameter's value. Given the estimate $\hat{y}$ of a grid variable and its variance $\mathrm{var}[\hat{y}]$, the corresponding CI is $CI_{\hat{y}}^{1-\alpha} = \left(\hat{y} \pm z_{1-\alpha/2}\sqrt{\mathrm{var}\left[\hat{y}\right]}\right)$ where $\alpha$ is the significance level, $z_{1-\alpha/2} = \Phi^{-1}(1-\alpha/2)$ the quantile of the standard normal distribution, with $\Phi$ its cumulative distribution function. The estimate of $x$ and its covariance matrix are given by $\mathrm{E}[\hat{x}] = A^{-1}b$ and $\mathrm{cov}[\hat{x}, \hat{x}^T] = A^{-1}$. The two include expected value and covariance of the primal and the dual variables of the optimization problem, depending on the LSE formulation. The covariance matrix for the primal variables $\mathrm{cov}[\hat{v}, \hat{v}^T]$ is extracted as in [24], by selecting the rows of $A^{-1}$ that correspond to the derivatives of the Lagrangian function with respect to $v$, and the columns of $A^{-1}$ that correspond to the variables $v$. For formulation (5), $\mathrm{cov}[\hat{v}, \hat{v}^T]$ corresponds to the sub-block of $A^{-1}$ associated with the $H_1^H \Omega_1^{-1} H_1$ block of $A$ in (6), whereas for formulation (7), it is located in the upper-left zero sub-block of $A^{-1}$ of (8). In rectangular coordinates $\mathrm{cov}[\hat{v}, \hat{v}^T] \in \mathbb{R}^{2n \times 2n}$ is

$$\mathrm{cov}[\hat{v}, \hat{v}^T] = \begin{bmatrix} \mathrm{cov}\left[\hat{v}_\Re, \hat{v}_\Re\right] & \mathrm{cov}\left[\hat{v}_\Re, \hat{v}_\Im\right] \\ \mathrm{cov}\left[\hat{v}_\Im, \hat{v}_\Re\right] & \mathrm{cov}\left[\hat{v}_\Im, \hat{v}_\Im\right] \end{bmatrix}. \quad (14)$$

The uncertainty of the real and imaginary parts of voltage estimates can be readily mapped into polar coordinates, of more practical use for operators and, similarly, to all their derived variables defining the grid's operating point.

### *D. Efficient algorithm for uncertainty quantification*

The challenge in developing a computationally efficient algorithm for online deployment, is obtaining the required estimate covariance entries from the inverse of matrix $A$. The LSE problem, hence the system of KKT conditions $Ax = b$, is typically solved using Cholesky or LU decomposition, which do not invert matrix $A$ as it is computationally expensive. The "sparse inverse algorithm" [25], calculates the values of the matrix inverse $A^{-1}$ only at the locations corresponding to the nonzero entries of the $L$ and $U$ triangular factors, and is therefore substantially faster than computing the entire inverse. While sufficient for LSE formulation (3), it is not suitable for (5) and (7). In particular, in the augmented formulation (7) (cf. Section III-C), the required entries of $A^{-1}$ lie in a zero block of $A$; the corresponding positions in $L$ and $U$ are also zero, and thus those inverse entries are not computed by the sparse inverse algorithm. Additionally, computing the variances of branch currents $[i_{ij}^{\Re}, i_{ij}^{\Im}]^\top = M_{ij}[v_i^{\Re}, v_j^{\Re}, v_i^{\Im}, v_j^{\Im}]^\top$ ($M_{ij}$ linear map) requires accessing the entries of $A^{-1}$ corresponding to the combinations of the real and imaginary parts of the bus voltages at the branch sending $i$ and receiving $j$ ends, according to $\mathrm{cov}[\sum_i a_i X_i, \sum_j b_j Y_j] = \sum_i \sum_j a_i b_j \,\mathrm{cov}[X_i, Y_j]$. To address this issue, this work proposes a procedure to efficiently compute *any* sparse subset of $A^{-1}$ using $L$ and $U$ triangular factors of $A$. The procedure is outlined in Algorithm 1, applicable to both real and complex matrices. The key aspects that distinguish it from the classical sparse inverse algorithm include

- identifying the combined sparsity pattern $S$, which ensures that all values of the desired sparse subset of $A^{-1}$ are

979-8-3315-8138-1

**Algorithm 1** Proposed sparse inverse subset computation

**Let**

- $A, L, U$ be sparse $k \times k$ matrices,
- $P, Q \in \{0,1\}^{k\times k}$ be permutation matrices of rows and columns of $A$, such that $LU = PAQ$,
- $S_d \in \{0,1\}^{k\times k}$ be the sparsity pattern of the desired subset of $A^{-1}$.

**Steps**

1: Create a modified version of $A$ such that its elements corresponding to the sparse inverse subset are guaranteed to be nonzero, and permute it: $A_m \leftarrow P \cdot (|A| + S_d) \cdot Q$.
2: Symmetrize the modified matrix: $A_m \leftarrow A_m + A_m^T$.
3: Permute the desired sparsity pattern: $S_d^{'} \leftarrow Q^T S_d P^T$.
4: Compute $R \in \{0,1\}^{k\times k}$, which is the sparsity pattern of the Cholesky factor of $A_m$, using symbolic factorization.
5: Create symmetric sparsity pattern: $S \leftarrow R \vee R^T$.
6: Combine $S$ with desired sparsity pattern: $S \leftarrow S \vee S_d^{'}$.
7: Identify sparsity pattern $S_r \in \{0,1\}^{k\times k}$, which is relevant for computing the desired sparse subset of permuted $A^{-1}$. Use $S$, $L$, and $U$ and right-looking updates.
8: Compute desired sparse subset $Z$ of permuted $A^{-1}$ from $S_r$, $L$, and $U$ using left-looking updates.
9: Permute the result back: $Z \leftarrow QZP$. This reverts $Z$ to the original indexing of $A^{-1}$.

**Output**

The sparse subset $Z$ of $A^{-1}$, corresponding to the desired sparsity pattern $S_d$.

computed;

- reducing $S$ to the relevant sparsity pattern $S_r$, which leads to the calculation of only necessary values for the desired sparse subset of $A^{-1}$, thus reducing the computation time.

The algorithm was implemented in C by modifying the standard sparse inverse routine from SuiteSparse [26]. A mex interface was developed to enable the algorithm to be called from Matlab.

## IV. Numerical Experiments

Regarding the simulation setup, numerical experiments were carried out in MATLAB using three test cases available in MATPOWER v8.0 [27], namely, the 118-bus (small), the 2869-bus (medium) and the 10k-bus (large) networks. The maximum magnitude and phase measurement errors were set, respectively, to $1\%$ of the measured magnitude and $1\,\mathrm{mrad}$; accordingly, their standard deviations $\sigma_Z$, $\sigma_\theta$ were set to $0.33\%$ and $0.33\,\mathrm{mrad}$. The experiments were executed on a computer equipped with an AMD Ryzen 3 7330U processor, clocked at $2.3\,\mathrm{GHz}$, and $16\,\mathrm{GB}$ of RAM.

### A. Accuracy and computation time

The performance of the proposed estimator 3 was evaluated in terms of its accuracy and computation time, as compared to the two conventionally used linear estimators 1 and 2:

1) "cmplx": complex coordinates, $\sigma_{\Re_i\Re_i} = \sigma_{\Im_i\Im_i}$ $\forall i$ and $\sigma_{\Re_i\Im_j} = 0$ $\forall i, j$.
2) "rect, no corr": rectangular coordinates, $\sigma_{\Re_i\Re_i} \neq \sigma_{\Im_i\Im_i}$ $\forall i$, and $\sigma_{\Re_i\Im_j} = 0$ $\forall i, j$ [1].
3) "rect, corr": rectangular coordinates, $\sigma_{\Re_i\Re_i} \neq \sigma_{\Im_i\Im_i}$, and $\sigma_{\Re_i\Im_j} \neq 0$ $\forall i = j$.

Accuracy was quantified using the $L_1$ norm $\|\hat{x} - x^{true}\|_1$ for magnitude and phase errors separately, with $\hat{x}$ estimated and $x^{true}$ true bus voltage magnitude or phase. The algorithm was run for numerous noise realizations, i.e. several noisy datasets were generated from the original noiseless measurements representing a steady-state feasible operating point. Figure 3 illustrates the errors are highest for estimator 1, and smallest for 3, with the difference being particularly pronounced for the phase errors. This demonstrates that properly accounting for the correlation between the real and imaginary parts of measurements significantly improves accuracy of the estimator.

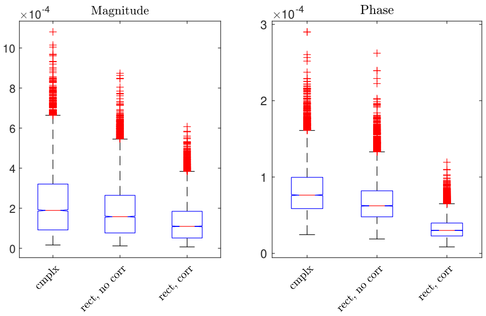


Fig. 3: Distribution of median (over the buses) magnitude and phase errors of state estimates, for $10,000$ noise realizations.

Figure 4 shows that the LSE solution times for the real-valued estimators are comparable (and approximately twice those of estimator 1, due to the doubled number of variables and equations) regardless of whether the correlation between the real and imaginary parts of the measurements is considered. Further, all estimators remain adequately fast even for large-scale systems.

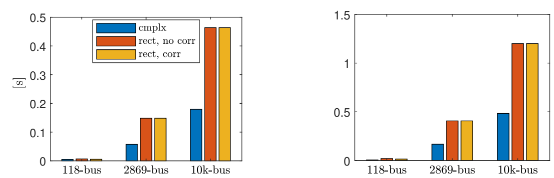


Fig. 4: LSE problem solution time. Constrained (5) (left), and augmented (7) (right) formulation.

### B. Uncertainty quantification of estimates and sparse inverse speed

Shaded rectangles in Figure 5 (left) illustrate the uncertainty of the obtained estimates for a representative nodal voltage in the 118-bus network, providing a visual example of the aggregate statistical trend in the right panel. Estimator 3 reduces the uncertainty in the estimated magnitude and phase by factors of 2 and 6 at maximum, respectively.

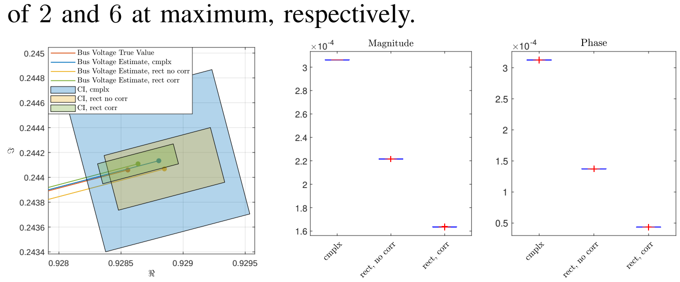


Fig. 5: Joint CIs for magnitude and phase of bus voltage estimates (left). Distribution of median (over the buses) variance of the estimates over $10,000$ noise realizations (right).

The statistical significance of the CIs was assessed through their coverage frequency, defined as the percentage of CIs

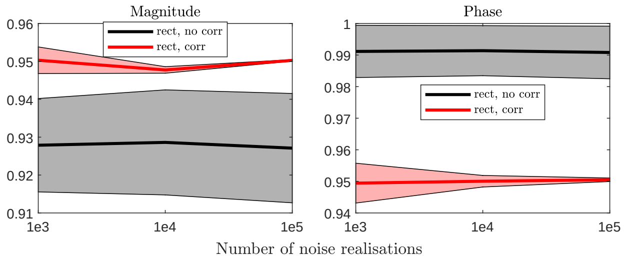


Fig. 6: Coverage frequency of CIs for magnitude and phase of bus voltage estimates as a function of the number of noise realizations, confidence level of 95%, 118-bus grid.

that actually contain the true bus voltages. Figure 6 shows the distribution of this metric as a function of the number of noise realizations. Notably, only the proposed estimator achieved a mean coverage frequency approaching 95%, with its standard deviation decreasing as the number of realizations increased. Figure 7 shows the computation time required to obtain the variance of the bus voltage estimates. Conventional algorithms for uncertainty quantification (left) are inefficient for formulation (7), particularly in large-scale grids. In contrast, the proposed sparsity-promoting approach (right) achieves computation times comparable to those of the LSE solution in Figure 4, making it suitable for real-time applications.

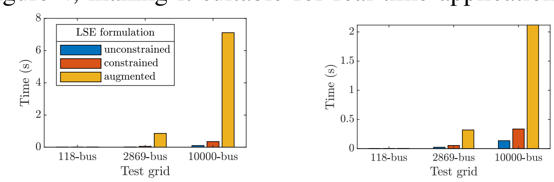


Fig. 7: Time for computation of variance of estimates. Without (left) and with (right) sparsity promotion.

## V. Conclusion

This paper proposes a general framework (a mathematical formulation and a solution algorithm with a MATLAB implementation) to solve LSE under a noise model with minimal approximations, grounded in experimentally characterized measurement-error statistics. Specifically, measurement uncertainty is modeled as independent Gaussian magnitude and phase errors with distinct standard deviations, which in rectangular coordinates induces a non-diagonal precision matrix. Although not new, this model is rarely used in practice due to its computational cost; the proposed approach overcomes this limitation through a dedicated sparse linear-algebra routine that makes it tractable in real time.

In addition to point estimates, the method computes their CIs, which can be propagated to derived quantities, e.g. branch currents. The underlying sparse inversion routine (enabling recovery of selected entries of a matrix inverse according to a prescribed sparsity pattern) is also applicable beyond SE. Comparative analyses against two commonly used linear estimators show that the proposed estimator is the only one delivering uncertainty quantification that is statistically consistent with the adopted noise model, while also improving accuracy and reducing estimate variances and without compromising speed. These results highlight the practical relevance of the method for grid monitoring and control.

## References

[1] M. Paolone, J.-Y. L. Boudec, S. Sarri, and L. Zanni, "Static and recursive pmu-based state estimation processes for transmission and distribution power grids," in 1st ed. London, UK, The Institution of Engineering and Technology - IET, 2015, ch. 6.

[2] A. Abur and A. G. Exposito, *Power system state estimation: theory and implementation*. CRC press, 2004.

[3] R. K. Gupta et al., "Learning power flow models and constraints from time-synchronized measurements: A review," *Proceedings of the IEEE*, vol. 112, no. 12, pp. 1799–1830, 2024.

[4] C. Laurano, P. A. Pegoraro, C. Sitzia, A. V. Solinas, S. Sulis, and S. Toscani, "Refined modeling and compensation of current transformers behavior for line parameters estimation based on synchronized measurements," *IEEE Open Journal of Instrumentation and Measurement*, vol. 2, pp. 1–11, 2023.

[5] P. A. Pegoraro, K. Brady, P. Castello, C. Muscas, and A. Von Meier, "Line impedance estimation based on synchrophasor measurements for power distribution systems," *IEEE Transactions on Instrumentation and Measurement*, vol. 68, no. 4, pp. 1002–1013, Apr. 2019.

[6] Y. Liao and M. Kezunovic, "Online optimal transmission line parameter estimation for relaying applications," *IEEE Transactions on Power Delivery*, vol. 24, no. 1, pp. 96–102, 2009.

[7] C. Mishra, V. A. Centeno, and A. Pal, "Kalman-filter based recursive regression for three-phase line parameter estimation using synchrophasor measurements," in *2015 IEEE Power & Energy Society General Meeting*, 2015, pp. 1–5.

[8] "Instrument transformers—part 1: General requirements," *IEC Standard 61869-1:2009*, 2009.

[9] "Ieee/iec international standard - measuring relays and protection equipment - part 118-1: Synchrophasor for power systems - measurements," *IEC/IEEE 60255-118-1:2018*, pp. 1–78, 2018.

[10] P. Castello, C. Muscas, and P. A. Pegoraro, "Statistical behavior of pmu measurement errors: An experimental characterization," *IEEE Open Journal of Instrumentation and Measurement*, vol. 1, pp. 1–9, 2022.

[11] L. Zanni, "Power-system state estimation based on pmus: Static and dynamic approaches - from theory to real implementation," Ph.D. dissertation, EPFL, 2017.

[12] C. Huang et al., "Power distribution system synchrophasor measurements with non-gaussian noises: Real-world data testing and analysis," *IEEE Open Access Journal of Power and Energy*, vol. 8, pp. 223–228, 2021.

[13] P. Castello, G. Gallus, C. Muscas, P. A. Pegoraro, D. Sitzia, and S. Sulis, "A statistical investigation of pmu errors in current measurements," in *2023 IEEE International Instrumentation and Measurement Technology Conference (I2MTC)*, 2023, pp. 1–6.

[14] K.-i. Nishiya, J. Hasegawa, and T. Koike, "Dynamic state estimation including anomaly detection and identification for power systems," 1982.

[15] G. Valverde and V. Terzija, "Unscented kalman filter for power system dynamic state estimation," *IET Generation, Transmission & Distribution*, vol. 5, pp. 29–37, 2011.

[16] E. Kyriakides and G. Heydt, "Calculating confidence intervals in parameter estimation: A case study," *IEEE Transactions on Power Delivery*, vol. 21, no. 1, pp. 508–509, 2006.

[17] Y. Guo, X. Zhou, C. Zhao, L. Chen, and T. H. Summers, "Optimal power flow with state estimation in the loop for distribution networks," *IEEE Systems Journal*, vol. 17, no. 3, pp. 3694–3705, 2023.

[18] A. Al-Othman and M. Irving, "Uncertainty modelling in power system state estimation," *IEE Proceedings - Generation, Transmission and Distribution*, vol. 152, no. 2, p. 233, 2005.

[19] A. Al-Othman and M. Irving, "Analysis of confidence bounds in power system state estimation with uncertainty in both measurements and parameters," *Electric Power Systems Research*, vol. 76, no. 12, pp. 1011–1018, Aug. 2006.

[20] Z. Khan, R. B. Razali, H. Daud, N. M. Nor, M. Fotuhi-Firuzabad, and K. L. Krebs, "The computation of confidence intervals for the state parameters of power systems," *SpringerPlus*, vol. 5, no. 1, p. 1943, Dec. 2016.

[21] X. Zhang, W. Yan, M. Huo, and H. Li, "Robust interval state estimation for distribution systems considering pseudo-measurement interval prediction," *Journal of Modern Power Systems and Clean Energy*, vol. 12, no. 1, pp. 179–188, 2024.

[22] A. Abur, *State estimation*, Course Lecture Notes, 2015.

[23] D. Lerro and Y. Bar-Shalom, "Tracking with debiased consistent converted measurements versus ekf," *IEEE Transactions on Aerospace and Electronic Systems*, vol. 29, no. 3, pp. 1015–1022, 1993.

[24] H. G. Bock, E. Kostina, and O. Kostyukova, "Covariance matrices for parameter estimates of constrained parameter estimation problems," *SIAM Journal on Matrix Analysis and Applications*, vol. 29, no. 2, pp. 626–642, 2007.

[25] Y. Campbell and T. Davis, "Computing the sparse inverse subset: An inverse multifrontal approach," Nov. 1995.

[26] *Suitesparse: A suite of sparse matrix software*, http://suitesparse.com.

[27] R. D. Zimmerman and C. E. Murillo-Sanchez, *Matpower (version 8.0)*, https://matpower.org, 2024.

979-8-3315-8138-1